Combined Effects of Shunt and Luminescence Coupling on External Quantum Efficiency Measurements of Multijunction Solar Cells

Jing-Jing Li, *Student Member, IEEE*, Swee Hoe Lim, *Member, IEEE*, Charles R. Allen, *Member, IEEE*, Ding Ding, and Yong-Hang Zhang, *Senior Member, IEEE*

***Abstract*—The combined effects of shunt and luminescence coupling on the measurement artifact of external quantum efficiency (EQE) of multi-junction solar cells are studied. The EQE measurement artifact is modeled using DC and small-signal equivalent circuits under voltage and light bias conditions. The modeling results are verified with EQE measurements of a Ge bottom cell of a triple-junction solar cell. It is found that the optimal bias light intensity to minimize the EQE measurement artifact is the result of the tradeoff between the shunt and the luminescence coupling effects.**

***Index Terms*—Luminescence coupling, multi-junction solar cells, quantum efficiency, shunt.**

I. Introduction

THE spectral external quantum efficiency (EQE) is of significant importance for the design and performance evaluation of multijunction solar cells [1], [2]. Because of their monolithic integration and series connection, the subcells are coupled both electrically and optically. Therefore, the EQE of the individual subcells is determined not only by their own properties, but by the interactions between them as well. It has been demonstrated that a low shunt resistance of a subcell can reduce the spectral response in its absorbing wavelength range, i.e., from its bandgap wavelength to that of the upper adjacent subcell with a larger bandgap, while giving rise to an erroneous response signal outside its absorbing wavelength range [3], [4]. Recently, it has been shown that the luminescence coupling from a subcell to the lower subcell with a smaller bandgap [5]–[7], or from a solar cell to a photodetector [8], can cause similar measurement artifacts. The presence of both shunt and luminescence coupling makes the characteristics of the artifact even more complicated.

To measure the EQE of a subcell, proper light bias has to be used to make that subcell current limiting. Moreover, the multijunction solar cell needs to be voltage biased if the subcell under test has a low shunt resistance, as is usually the case for the Ge subcell. Note that the EQE measurement artifact depends strongly on both the voltage and light biases, which change the operating conditions of the subcells. For the EQE measurement of the Ge bottom cell of a triple-junction solar cell, the voltage bias predominantly controls the operating point of the reverse-biased Ge bottom cell; therefore, it is most effective to correct the measurement artifact due to the Ge shunt resistance. On the other hand, the light bias on the InGaAs middle cell predominantly controls the operating point of the forward-biased InGaAs middle cell, whereas the operating point of the reverse-biased Ge bottom cell is not changed as much as in the case of voltage bias. The light bias, therefore, allows the control of luminescence coupling from the InGaAs middle cell to the Ge bottom cell. Using proper voltage and light biases thus offers the flexibility to access the individual effect of shunt or luminescence coupling on the measurement artifact.

In this paper, the voltage and light biases are used to study the combined effects of shunt and luminescence coupling on EQE measurements of triple-junction solar cells.

II. Experiments

EQE measurements are performed on high-performance commercial InGaP/InGaAs/Ge triple-junction solar cells. The measurement setup (Newport QE/IPCE) consists of a broadband light source chopped at 30 Hz, a monochromator, and a lock-in amplifier. A 405-nm laser diode is set at an intensity that is high enough to saturate the InGaP top cell, while the intensity of a 780-nm laser diode is turned up gradually to increase the photocurrent I_{BS}^{M} generated in the InGaAs middle cell. I_{BS}^{M} is measured prior to the EQE measurements using an additional 980-nm laser diode to saturate the Ge bottom cell. Fig. 1 shows the measurement artifact of higher than expected EQE in the InGaAs response range from 670 to 880 nm and lower than expected EQE in the Ge response range above 880 nm. In order to demonstrate the Ge shunt effect, the triple-junction solar cell is reverse biased at -0.45 V rather than the optimal bias voltage that minimizes the shunt effect. It can be seen in Fig. 1 that the measurement artifact is minimized at the photocurrent I_{BS}^{M} of 2.5 mA, and it becomes more severe as I_{BS}^{M} decreases or increases. The enhanced artifact for smaller and larger I_{BS}^{M} can be explained by the low shunt resistance of the Ge subcell and the luminescence coupling between the InGaAs and Ge subcells,

Manuscript received July 18, 2011; revised September 27, 2011; accepted October 7, 2011. Date of publication November 28, 2011; date of current version December 27, 2011. This work was supported in part by the Science Foundation Arizona under Contract SRG 0190-07 and Contract SRG 0339-08, the Air Force Research Laboratory/Space Vehicles Directorate under Contract FA9453-08-2-0228, a National Science Foundation Grant under Contract 1002114, and by Newport Corporation.

The authors are with the Center for Photonics Innovation and the School of Electrical, Computer and Energy Engineering, Arizona State University, Tempe, AZ 85287 USA (e-mail: Jingjing.Li@asu.edu; slim20@asu.edu; c.allen@asu.edu; dding@asu.edu; yhzhang@asu.edu).

Color versions of one or more of the figures in this paper are available online at http://ieeexplore.ieee.org.

Digital Object Identifier 10.1109/JPHOTOV.2011.2172188

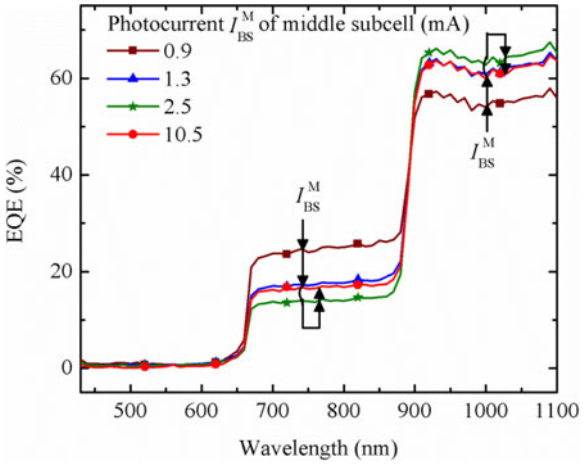

Fig. 1. EQE spectra of the Ge bottom cell of a triple-junction solar cell at the reverse-bias voltage of −0.45 V and under different bias light intensities and photocurrents $I_{\rm BS}^{M}$ generated in the InGaAs middle cell.

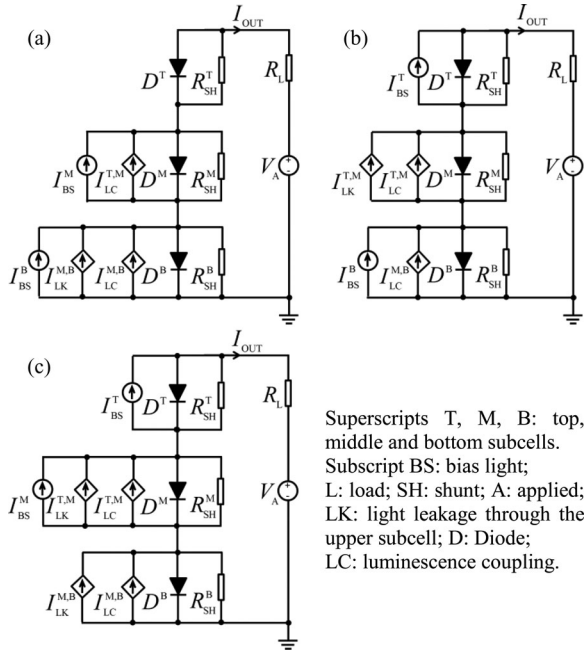

Fig. 2. DC equivalent circuits of a triple-junction solar cell at the voltage and light bias conditions of EQE measurements for (a) the top subcell, (b) middle subcell, and (c) bottom subcell.

respectively, as will be discussed later. Consequently, the optimal bias light intensity on the InGaAs middle cell, at which the measurement artifact of the Ge bottom cell is minimized, is determined by the combined effects of shunt and luminescence coupling.

III. Theory

A. DC Model

Fig. 2(a)–(c) show the circuit representations of the triple-junction solar cell under the dc voltage and light bias conditions for the EQE measurement of the top, middle, and bottom subcell, respectively. The current sources $I_{\rm BS}^{T}$, $I_{\rm BS}^{M}$, and $I_{\rm BS}^{B}$ are the photocurrents generated by the intentional light biases on the three subcells. Because the bias light on an upper subcell may not be absorbed completely, additional photocurrent can be generated in the lower subcell by the unabsorbed bias light. This leakage current is modeled by the current-controlled current source $I_{\rm LK}^{T,M}=\alpha_{\rm LK}^{T,M}I_{\rm BS}^{T}$ from the top to the middle subcell and $I_{\rm LK}^{M,B}=\alpha_{\rm LK}^{M,B}I_{\rm BS}^{M}$ from the middle to the bottom subcell, respectively, with the leakage strengths $\alpha_{\rm LK}^{T,M}$ and $\alpha_{\rm LK}^{M,B}$. Moreover, the radiative recombination in an upper subcell with a larger bandgap generates photons that can be reabsorbed in the lower subcell. This luminescence coupling is modeled by the current-controlled current source $I_{\rm LC}^{T,M}=f_{\rm LC}^{T,M}(I(D^{T}))$ from the top to the middle subcell and $I_{\rm LC}^{M,B}=f_{\rm LC}^{M,B}(I(D^{M}))$ from the middle to the bottom subcell, respectively. Note that the light leakage and luminescence coupling are only considered for adjacent subcells. The voltage source $V_{\rm A}$ is used to control the effects of shunt resistances $R_{\rm SH}^{T}$, $R_{\rm SH}^{M}$, and $R_{\rm SH}^{B}$.

B. Small-Signal Model

Under proper voltage and light biases, the EQE spectrum of the subcell under test is measured by scanning the wavelength of the AC monochromatic light. Fig. 3(a)–(c) show the small-signal equivalent circuits of the triple-junction solar cell when the photocurrent $i_{\rm ph}$ is generated by the monochromatic light in the absorbing wavelength range of the top, middle, and bottom subcells, respectively. The leakage currents are modeled as $i_{\rm lk}^{t,m}=\alpha_{\rm lk}^{t,m}i_{\rm ph}$ and $i_{\rm lk}^{m,b}=\alpha_{\rm lk}^{m,b}i_{\rm ph}$. The luminescence coupling currents are modeled as $i_{\rm lc}^{t,m}=\alpha_{\rm lc}^{t,m}i(r_d^{t})$ and $i_{\rm lc}^{m,b}=\alpha_{\rm lc}^{m,b}i(r_d^{m})$, where $\alpha_{\rm lc}^{t,m}$ and $\alpha_{\rm lc}^{m,b}$ are the small-signal luminescence coupling strengths. The load resistor $R_{\rm L}$ is used to adjust the bias voltage on the solar cell. The EQE measurement artifact comes from the fact that the measured output current $i_{\rm out}$ is not always the same as the photocurrent $i_{\rm ph}$ generated by the subcell under test. The relation between $i_{\rm out}$

$$\frac{i_{\rm out}}{i_{\rm ph}}=\frac{(r^{t}//r_{\rm sh}^{t})+\left(\gamma^{t,m}+\alpha_{\rm lk}^{t,m}\right)(r^{m}//r_{\rm sh}^{m})+\left(\gamma^{t,m}+\alpha_{\rm lk}^{t,m}\right)\gamma^{m,b}\left(r^{b}//r_{\rm sh}^{b}\right)}{(r^{t}//r_{\rm sh}^{t})+(1+\gamma^{t,m})(r^{m}//r_{\rm sh}^{m})+\left[1+(1+\gamma^{t,m})\gamma^{m,b}\right]\left(r^{b}//r_{\rm sh}^{b}\right)+R_{L}} \tag{1}$$

$$\frac{i_{\rm out}}{i_{\rm ph}}=\frac{(r^{m}//r_{\rm sh}^{m})+\left(\gamma^{m,b}+\alpha_{\rm lk}^{m,b}\right)\left(r^{b}//r_{\rm sh}^{b}\right)}{(r^{t}//r_{\rm sh}^{t})+(1+\gamma^{t,m})(r^{m}//r_{\rm sh}^{m})+\left[1+(1+\gamma^{t,m})\gamma^{m,b}\right]\left(r^{b}//r_{\rm sh}^{b}\right)+R_{L}} \tag{2}$$

$$\frac{i_{\rm out}}{i_{\rm ph}}=\frac{\left(r^{\rm b}//r_{\rm sh}^{\rm b}\right)}{(r^{\rm t}//r_{\rm sh}^{\rm t})+(1+\gamma^{\rm t,m})(r^{\rm m}//r_{\rm sh}^{\rm m})+\left[1+(1+\gamma^{\rm t,m})\gamma^{\rm m,b}\right]\left(r^{\rm b}//r_{\rm sh}^{\rm b}\right)+R_{L}} \tag{3}$$

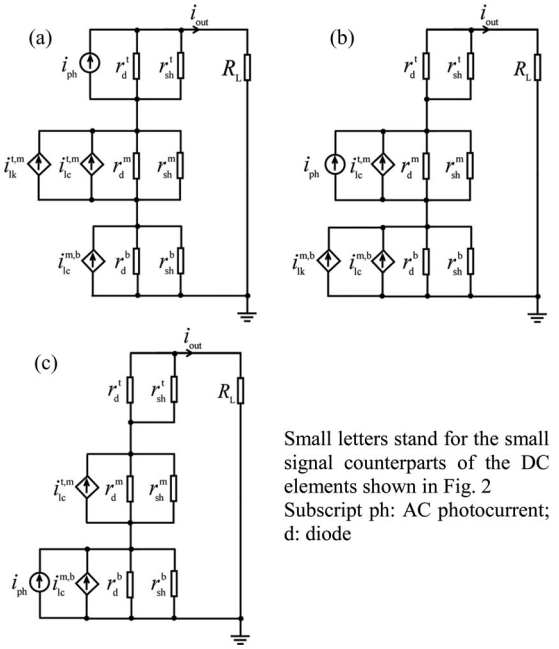

Fig. 3. Small-signal equivalent circuits of a triple-junction solar cell when the wavelength of the ac monochromatic light in EQE measurements is in the wavelength range of the (a) top subcell, (b) middle subcell, and (c) bottom subcell.

and $i_{\rm ph}$ is used as a measure of the EQE measurement artifact. Equations (1)–(3), shown at the bottom of the previous page, show $i_{\rm out}/i_{\rm ph}$ in the absorbing wavelength range of the top, middle, and bottom subcell, respectively, derived from the circuits in Fig. 3(a)–(c), where $\gamma^{t,m} = \alpha_{\rm lc}^{t,m} r_{\rm sh}^t/(r^t + r_{\rm sh}^t)$, $\gamma^{m,b} = \alpha_{\rm lc}^{m,b} r_{\rm sh}^m/(r^m + r_{\rm sh}^m)$, and $r^t//r_{\rm sh}^t$, $r^m//r_{\rm sh}^m$, and $r^b//r_{\rm sh}^b$ are the parallel resistances of the small-signal diode resistance and shunt resistance of the top, middle, and bottom subcell, respectively. The small-signal luminescence coupling strengths and small-signal resistances depend on the operating points of the subcells. According to the small-signal approximation, they can be expressed as

$$\alpha_{\rm lc} = \left.\frac{dI_{\rm LC}}{dI\,({\rm D})}\right|_{V_{\rm subcell}} \tag{4}$$

$$r = \left.\frac{dV}{dI}\right|_{V_{\rm subcell}}. \tag{5}$$

The light leakage depends more on the subcell thickness and material quality; therefore, the leakage strength $\alpha_{\rm lk}$ is a constant at a certain wavelength.

IV. Characterization

A. Small-Signal Luminescence Coupling Strength and Leakage Strength

The small-signal luminescence coupling strengths and the leakage strengths in (1)–(3) are characterized by probing the luminescence of the subcells [7], [9]. The radiative recombination in a subcell generates photons with the energy at the bandgap of the subcell. These photons either escape from the solar cell surface generating luminescence L, or emit into the lower subcell with a smaller bandgap and are reabsorbed there. The relationship between the number of photons emitted into the free space and the number being reabsorbed, as shown in (6) below, is characteristic of the solar cell at a given set of voltage and light biases

$$\int \frac{L\,(\lambda)\,\lambda}{hc} d\lambda = \frac{\chi}{q} I_{\rm LC} \tag{6}$$

where the parameter χ depends on the geometries and refractive indices of the two subcells and the internal quantum efficiency of the lower subcell. In luminescence measurements, χ is further scaled according to the solid angle and responsivity of the detector. From (4) and (6), the small-signal luminescence coupling strength is obtained as

$$\alpha_{\rm lc} = \frac{dI_{\rm LC}}{dI\,({\rm D})} = \frac{d\left(q\int \frac{L(\lambda)\lambda}{hc} d\lambda \Big/ \chi\right)}{dI({\rm D})}. \tag{7}$$

The luminescence intensity L in (7) is measured using a fiber-coupled radiometer (EPP2000), while the bias light intensity on the InGaAs middle cell is varied. The recombination current I(D) in (7) is determined as the photocurrent of the InGaAs subcell subtracted by the output current of the triple junction.

In order to minimize the shunt effect and isolate the luminescence coupling effect, the triple-junction solar cell is forward biased at the optimal voltage of 0.2 V, at which the small-signal resistance of the Ge subcell is the largest. The optimal bias voltage usually does not change much with the bias light intensity when the luminescence coupling is dominant. The triple-junction solar cells used in this study only have luminescence coupling between the InGaAs and Ge subcells. Furthermore, at the optimal bias voltage, the shunt resistances can be neglected. Therefore, (2) and (3) are simplified as

$$\frac{i_{\rm out}}{i_{\rm ph}} = \frac{\alpha_{\rm lc}^{\rm m,b} + \alpha_{\rm lk}^{\rm m,b}}{1 + \alpha_{\rm lc}^{\rm m,b}} \tag{8}$$

$$\frac{i_{\rm out}}{i_{\rm ph}} = \frac{1}{1 + \alpha_{\rm lc}^{\rm m,b}}. \tag{9}$$

$i_{\rm out}/i_{\rm ph}$ in (8) and (9) can then be determined by plugging in $\alpha_{\rm lc}^{m,b}$ from EL measurements as shown in Fig. 4, with the parameters χ and $\alpha_{\rm lk}^{m,b}$ determined by fitting (8) and (9) with the EQE measurements. $i_{\rm ph}$ are taken as the best signals in the EQE measurements at the corresponding wavelengths. The slight deviations of the fitting at the smallest $I_{\rm BS}^M$ are because of the remaining shunt effect at the optimal voltage bias. The leakage strength $\alpha_{\rm lk}^{m,b}$ is determined as 5.5% at 780 nm from the fitting, and the small-signal luminescence coupling strength is calculated from the luminescence coupling current $I_{\rm LC}^{M,B}$ shown in the inset of Fig. 4. The small-signal luminescence coupling strength increases with the recombination current in the InGaAs subcell, because of the increased radiative recombination efficiency [7].

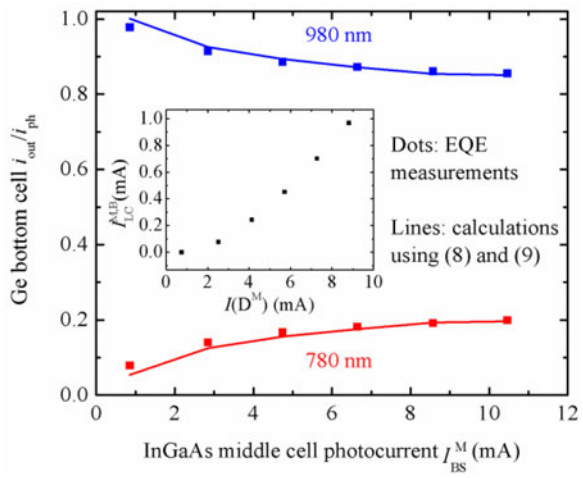

Fig. 4. Fitting of $i_{\rm out}/i_{\rm ph}$ of the Ge bottom cell obtained from EQE measurement (dots) with those from calculations (lines) using (8) and (9) at the optimal bias voltage of 0.2 V (forward bias) when the InGaAs photocurrent $I_{\rm BS}^{M}$ is increased. The inset shows the luminescence coupling current $I_{\rm LC}^{M,B}$ from the InGaAs middle cell to the Ge bottom cell versus the recombination current $I(\mathrm{D}^{M})$ of the InGaAs middle cell.

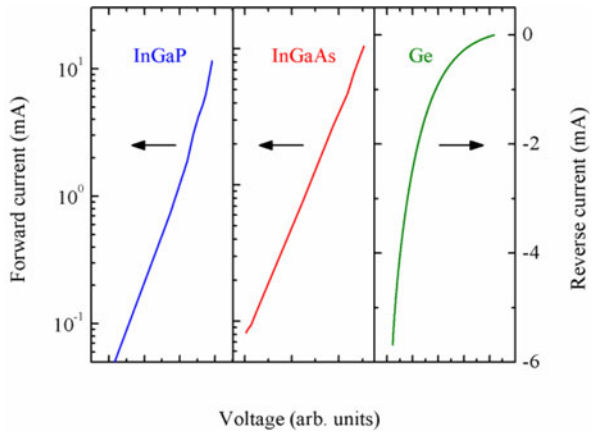

Fig. 5. Measured forward dark *I–V* curves of the InGaP and InGaAs subcells and reverse dark *I–V* curve of the Ge subcell.

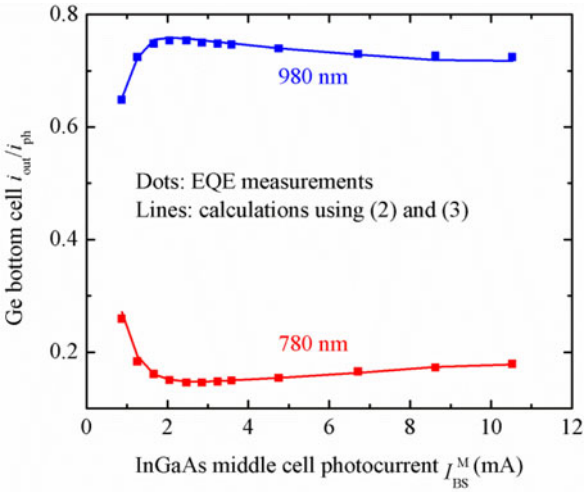

Fig. 6. $i_{\rm out}/i_{\rm ph}$ extracted from Fig. 1 (dots) and calculated using (2) and (3) (lines).

B. Small-Signal Resistance

The small-signal resistances are obtained from the subcell *I–V* curves using (5). Under the bias condition of EQE measurement of the Ge subcell, the InGaP and InGaAs subcells are forward biased, while the Ge subcell is reverse biased. The forward dark *I–V* curves of the InGaP and InGaAs subcells shown in Fig. 5 are obtained using the $I_{\rm sc}$–$V_{\rm oc}$ method [4]. The reverse dark *I–V* of the Ge subcell in Fig. 5 is obtained from a reverse voltage sweep when the InGaP and InGaAs subcells are light biased. During the measurement, the Ge subcell is light biased by the leakage light and luminescence coupled from the InGaAs subcell. Since the Ge reverse *I–V* obeys the superposition principle as observed in the measurements, the reverse dark *I–V* of the Ge subcell is obtained by subtracting the photocurrents from the measured current. The photocurrent from the leakage light is a constant under a certain light bias, while the photocurrent from the luminescence coupling varies with the bias voltage. The luminescence coupling current as a function of bias voltage or recombination current of the InGaAs subcell is calculated from the inset of Fig. 4, and is subtracted from the current measured at the corresponding voltage. The rest of the photocurrent is attributed to the leakage light. The voltage of Ge subcell is obtained by subtracting the voltages of the top two subcells from the measured voltage. It can be seen in Fig. 5 that the Ge reverse *I–V* curve shows a soft breakdown. The small-signal resistances are then determined from the slopes of the subcell *I–V* curves at the current measured under the voltage and light biases. Note that the subcell voltages are not accurately determined from the aforementioned procedure; therefore, they are left in arbitrary units in Fig. 5.

V. Results

Fig. 6 compares $i_{\rm out}/i_{\rm ph}$ extracted from Fig. 1 (dots) and calculated using (2) and (3) (lines). It can be seen in Fig. 6 that $i_{\rm out}/i_{\rm ph}$ increases and then decreases with $I_{\rm BS}^{M}$ when the ac monochromatic light is at 980 nm, and the trend is opposite when the ac monochromatic light is at 780 nm. When $I_{\rm BS}^{M}$ decreases, the InGaAs middle cell becomes less forward biased, and its small-signal resistance becomes comparable with the shunt resistance of the Ge bottom cell, which makes the artifact become worse. When $I_{\rm BS}^{M}$ increases, the voltage as well as the radiative recombination efficiency of InGaAs middle cell increases, which also makes the artifact become worse. The EQE measurement artifact is minimized at the optimal bias light intensity when $i_{\rm out}/i_{\rm ph}$ reaches the maximum at 980 nm and the minimum at 780 nm. It is dominated by the shunt effect at smaller bias light intensity and by the luminescence coupling effect at larger bias light intensity. The EQE measurement artifact of the Ge bottom cell is reproduced using (2) and (3) and the characterization methods developed in the previous section. A good agreement is found between the measurement and calculation results, as shown in Fig. 6.

VI. Discussions

In general, not every multijunction solar cell has all the characteristics of shunt and luminescence coupling in its subcells.

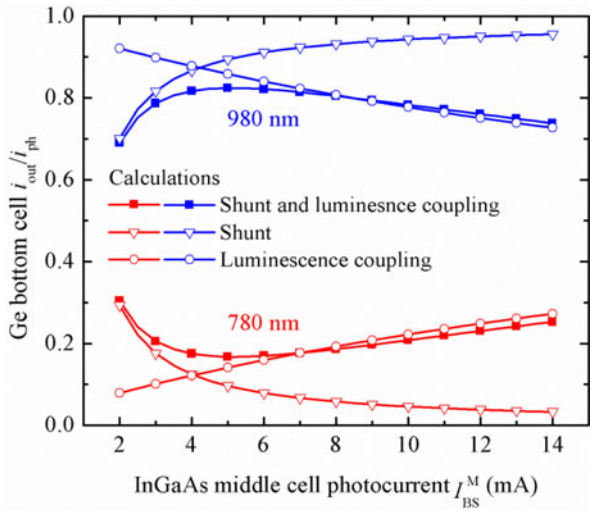

Fig. 7. Calculated $i_{\rm out}/i_{\rm ph}$ of Ge bottom cell at 980 and 780 nm with shunt and luminescence coupling (squares), with only shunt (open triangles) and only luminescence coupling (open dots) when the InGaAs photocurrent $I_{\rm BS}^{M}$ is increased.

TABLE I
PARAMETERS USED IN CALCULATIONS FOR FIG. 7

$I_{0\rm InGaP}$ (mA)	4.16×10^{-10}	$I_{\rm BS}^{\rm M}$ (mA)	2–14
$n_{\rm InGaP}$	2	$V_{\rm A}$ (V)	1.2 (reverse biased)
$I_{0\rm InGaAs}$ (mA)	8×10^{-6}	$\alpha_{\rm lk}$	0
$n_{\rm InGaAs}$	2	$\alpha_{\rm lc}^{\rm t,m}$	0
$I_{0\rm Ge}$ (mA)	1.6×10^{-4}	$\alpha_{\rm lc}^{\rm m,b}$	$15I(\rm D^M)^2$ (0 for shunt alone)
$n_{\rm Ge}$	1	$R_{\rm SH}^{\rm T}$ (Ω)	10^{10}
$R_{\rm L}$ (Ω)	1	$R_{\rm SH}^{\rm M}$(Ω)	10^{10}
$I_{\rm BS}^{\rm T}$ (mA)	10	$R_{\rm SH}^{\rm B}$(Ω)	$10^6 exp[2.1V(\rm D^B)]$ (10^{10} for only luminescence coupling)

Subcells with good material qualities have large shunt resistances and perhaps strong luminescence coupling as well. Subcells with poor material qualities have low shunt resistances and may be weak luminescence coupling. For special structures, such as the bifacial triple-junction solar cells, the upper two subcells are grown on the opposite side of the wafer from the bottom subcell; therefore, there is no luminescence coupling from the middle to the bottom subcell [10]. Equations (1)–(3) can be simplified for these special cases.

Fig. 7 compares the EQE measurement artifact caused by both shunt and luminescence coupling and the cases when there is only shunt or luminescence coupling. The calculations are done using SPICE with assumed subcell parameters shown in Table I. At small $I_{\rm BS}^{M}$, it can be seen that $i_{\rm out}/i_{\rm ph}$ accounting for both shunt and luminescence coupling (squares) follows those with only shunt (open triangles), indicating that the shunt effect dominates. As $I_{\rm BS}^{M}$ increases, the shunt effect is reduced (open triangles), because the small-signal resistance of the InGaAs middle cell decreases rapidly and the small-signal resistance of the Ge bottom cell becomes dominant. At large $I_{\rm BS}^{M}$, $i_{\rm out}/i_{\rm ph}$ because of both effects follow those with only luminescence coupling (open dots), indicating that the luminescence coupling dominates. Note that the luminescence coupling effect is slightly enhanced when the shunt effect is absent (open dots) at large $I_{\rm BS}^{M}$. This is because the small-signal resistance of the Ge bottom cell becomes larger with increased shunt resistance, and the InGaAs middle cell becomes more forward biased and generates stronger luminescence coupling to the Ge bottom cell. The tradeoff between shunt and luminescence coupling effects determines the optimal bias light intensity on the InGaAs middle cell that minimizes the EQE measurement artifact of the Ge bottom cell.

In addition, the sum of $i_{\rm out}/i_{\rm ph}$ in (1)–(3) is equal to 1 if R_L and $\alpha_{\rm lk}$ are negligible. For subcells with measurement artifact that cannot be eliminated using voltage and light biases, this unity rule provides a means to recover its true EQE, given that the true EQE of the other subcells can be obtained. A similar result has been obtained for shunt-induced EQE measurement artifact [6].

VII. CONCLUSION

In conclusion, the EQE measurement artifact originates from the electrical and optical interaction between subcells. It can be varied using voltage and light biases. To interpret EQE measurement results under the bias conditions and the monochromatic light scan, dc and small-signal equivalent models are developed for triple-junction solar cells. Characterization methods for the small-signal luminescence coupling strength, the leakage strength, and small-signal resistances in the models are demonstrated. A good agreement between the modeling and EQE measurement results is obtained for a Ge bottom cell. To minimize the EQE measurement artifact of the Ge bottom cell, the optimal bias light intensity on the InGaAs middle cell is determined from the tradeoff between the shunt and luminescence coupling effects, as confirmed by both measurement and modeling results. The modeling result also provides a guideline to recover the true EQE, if the measurement artifact cannot be eliminated by varying the voltage and light biases.

REFERENCES

[1] R. R. King, D. C. Law, K. M. Edmondson, C. M. Fetzer, G. S. Kinsey, H. Yoon, D. D. Krut, J. H. Ermer, R. A. Sherif, and N. H. Karam, "Advances in high-efficiency III-V multijunction solar cells," *Adv. Optoelectron.*, vol. 2007, pp. 1–9, 2007.

[2] U. Rau, "Reciprocity relation between photovoltaic quantum efficiency and electroluminescent emission of solar cells," *Phys. Rev. B*, vol. 76, no. 8, pp. 085303-1–085303-8, 2007.

[3] M. Meusel, C. Baur, G. Létay, A. W. Bett, W. Warta, and E. Fernandez, "Spectral response measurements of monolithic GaInP/Ga (In) As/Ge triple-junction solar cells: Measurement artifacts and their explanation," *Prog. Photovoltaics: Res. Appl.*, vol. 11, no. 8, pp. 499–514, Dec. 2003.

[4] S. H. Lim, K. O'Brien, E. H. Steenbergen, J.-J. Li, D. Ding, and Y.-H. Zhang, "Analysis of spectral photocurrent response from multijunction solar cells under variable voltage bias," in *Proc. 35th IEEE Photovoltaic Spec. Conf.*, 2010, pp. 712–716.

[5] H. Yoon, R. R. King, G. S. Kinsey, S. Kurtz, and D. D. Krut, "Radiative coupling effects in GaInP/GaAs/Ge multijunction solar cells," in *Proc. 3rd World Conf. Photovoltaic Energy Convers.*, 2003, pp. 745–748.

[6] G. Siefer, C. Baur, and A. W. Bett, "External quantum efficiency measurements of germanium bottom subcells: Measurement artifacts and

correction procedures," in *Proc. 35th IEEE Photovoltaic Spec. Conf.*, 2010, pp. 704–707.
[7] S. H. Lim, J.-J. Li, E. H. Steenbergen, and Y.-H. Zhang, "Luminescence coupling effects on multi-junction solar cell external quantum efficiency measurement," *Prog. Photovoltaics Res. Appl.*, in press.
[8] C. Baur, M. Hermle, F. Dimroth, and A. W. Bett, "Effects of optical coupling in III-V multilayer systems," *Appl. Phys. Lett.*, vol. 90, pp. 192109-1–192109-3, 2007.
[9] C. R. Allen, S. H. Lim, J.-J. Li, and Y.-H. Zhang, "Simple method for determining luminescence coupling in multi-junction solar cells," in *Proc. 37th IEEE Photovoltaic Spec. Conf.*, 2011, in press.
[10] P. T. Chiu, S. J. Wojtczuk, X. Zhang, C. Harris, and M. Timmons, "World record 42.3% efficient InGaP/GaAs/InGaAs concentrators using bifacial epigrowth," in *Proc. 37th IEEE Photovoltaic Spec. Conf.*, 2011, in press.

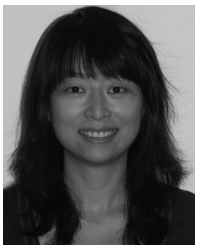

Jing-Jing Li (S'11) received the B.E. and M.S. degrees in electronic science and technology from Xi'an Jiaotong University, Xi'an, China, in 2004 and 2007, respectively. She is currently working toward the Ph.D. degree in electrical engineering with Arizona State University, Tempe.

Her current research interests are in compound semiconductors such as solar cells, light-emitting diodes, and photodetectors.

Swee Hoe Lim (M'03) received the B.S. degree in electrical and computer engineering from Cornell University, Ithaca, NY, in 2003 and the M.S. degree and Ph.D. degrees in electrical engineering from the University of California, San Diego, in 2006 and 2009, respectively.

From 2009 to 2011, he was a Postdoctoral Scholar with Arizona State University, Center for Photonics Innovation, before joining Nanosolar, Inc., San Jose, CA.

Charles R. Allen (M'10) received the B.S. degree from the School of Electrical and Computer Engineering, Purdue University, West Lafayette, IN, with a minor in physics in December 2004. He received the Ph.D. degree from the School of Electrical and Computer Engineering, Purdue University.

As a graduate student, he was a research assistant with the Birck Nanotechnology Center. He is a member of the IEEE Photonics Society; the IEEE Electron Device Society; the Minerals, Metals, and Materials Society; and Eta Kappa Nu. His research interests are in the areas of compound semiconductor devices, solar cells, and renewable energy.

Ding Ding received the Ph.D. degree in material science and engineering from Arizona State University (ASU), Tempe, in 2007.

He is currently an Assistant Research Scientist with the ASU MBE Optoelectronics Group, Center for Photonics Innovation and Department of Electrical Engineering, in the area of II–VI and III–V semiconductor material growth and characterization and their related optoelectronic devices, including multijunction solar cells and light-emitting diodes.

Yong-Hang Zhang (SM'09) received the B.S. and M.S. degrees in China, did research with the Max Planck Institute for Solid States, and received the doctoral degree in physics from the University of Stuttgart, Stuttgart, Germany, in 1991.

He was an Assistant Research Engineer with the University of California at Santa Barbara before he joined Hughes Research Labs in 1993. In 1996, he was appointed Associate Professor with the Department of Electrical Engineering with Arizona State University (ASU), Tempe, and was then promoted to Full Professor in 2000. He is currently the founding director of the Center for Photonics Innovation and a Professor in electrical engineering with the School of Electrical, Computer, and Energy Engineering, ASU. His areas of research interest include MBE growth, optical properties of semiconductor heterostructures, optoelectronic devices, and their applications. He has edited three conference proceedings and is the author or co-author of 184 publications in peer-reviewed journals and proceedings and 48 invited and over 200 contributed conference presentations, and has four issued U.S. patents. He has graduated and supervised 31 M.S. and Ph.D. students and 29 postdoctoral researchers and visiting scholars. More information about his group can be found on the webpage http://asumbe.eas.asu.edu/.